*Science & Technology Development Journal – Engineering and Technology 2023, 5(SI2):87-98*

Open Access Full Text Article

***Research Article***

# Free Vibration Analysis of Curved Shell Structures with Various Boundary Conditions by Using A Meshfree Method

**Thien Tich Truong[1,2,*], Vay Siu Lo[1,2,*]**

**ABSTRACT**

In this paper, the free vibration of curved shell structures with various boundary conditions is examined by using a meshfree method. The meshfree method in this study is based on the radial point interpolation method (RPIM). The RPIM shape function is chosen because it satisfies the Kronecker delta property allowing for the direct imposition of essential boundary conditions. The field variables and the geometry of the curved shell are interpolated through the RPIM shape function. The curved shell formulation is constructed based on the first-order shear deformation theory (FSDT), which considers the transverse shear strain. In a meshfree approach to investigate curved shell structures, a convected coordinate system is employed. This convected coordinate system is tied to the curved surface and used to map an arbitrary curved shell in 3D space into 2D space. To obtain the numerical solution, the calculation is performed first in this convected coordinate system and then mapped back to the global coordinate system. The accuracy and ability of the meshfree method have been shown through many numerical examples. The natural frequencies of curved shells with different geometry and boundary conditions are in good agreement with other available reference solutions.

**Key words:** free vibration analysis, curved shell, FSDT, meshfree method

*[1]Department of Engineering Mechanics, Faculty of Applied Sciences, Ho Chi Minh City University of Technology (HCMUT), 268 Ly Thuong Kiet Street, District 10, Ho Chi Minh City, Vietnam.*

*[2]Vietnam National University Ho Chi Minh City, Linh Trung Ward, Thu Duc City, Ho Chi Minh City, Vietnam.*

**Correspondence**

**Thien Tich Truong**, Department of Engineering Mechanics, Faculty of Applied Sciences, Ho Chi Minh City University of Technology (HCMUT), 268 Ly Thuong Kiet Street, District 10, Ho Chi Minh City, Vietnam.

Vietnam National University Ho Chi Minh City, Linh Trung Ward, Thu Duc City, Ho Chi Minh City, Vietnam.

Email: tttruong@hcmut.edu.vn

**Correspondence**

**Vay Siu Lo**, Department of Engineering Mechanics, Faculty of Applied Sciences, Ho Chi Minh City University of Technology (HCMUT), 268 Ly Thuong Kiet Street, District 10, Ho Chi Minh City, Vietnam.

Vietnam National University Ho Chi Minh City, Linh Trung Ward, Thu Duc City, Ho Chi Minh City, Vietnam.

Email: losiuvay@hcmut.edu.vn

## INTRODUCTION

Shell structures are commonly used in a variety of engineering applications, such as aerospace, marine, mobility and civil engineering. An important issue in engineering design is the free vibration behavior of the structures. The natural frequencies and mode shapes of a shell structure can be used to predict its dynamic response to external loads such as resonant. Therefore, analysis of the free vibration of thin shell structures is essential. The free vibration analysis of curved shell structures is discussed in [1–10]. Numerical methods for analyzing shell structures often use the first-order shear deformation theory (FSDT) [11–14] to describe the shell behavior because of its simple formulation.

Meshfree method is a genre of numerical methods that a mesh is not needed to define the discrete model of the domain of interest. This makes them well-suited for problems with irregular geometries or moving boundaries. One of the most well-known and earliest meshfree methods is the Element-Free Galerkin (EFG) method [15]. Many other meshfree methods can be listed as the Reproducing Kernel Particle Method (RKPM) [16], the Moving Kriging method (MK) [17,18], and the Radial Point Interpolation method (RPIM) [19,20]. The RPIM is a meshfree method that has the Kronecker delta property. This property enables RPIM to impose essential boundary conditions directly, which is not possible for other meshfree methods. Radial bases and polynomial bases are used to construct RPIM shape functions.

There are two main approaches to analyzing shell structures using meshfree methods. The first way is based on the exact shell model [21,22]. The second approach is the 3D degenerate shell element theory. The EFG method based on the 3D degenerate shell element theory is used by Noguchi et al. [23] to analyze the geometric nonlinearity of shells. Dai [24] and Peng [25] used the same approach for fracture analysis of curved shell structures. Chen [26] and Sadamoto [27–29] investigate the linear static and dynamic behavior, and even geometrically nonlinear analysis of curved shells.

A convected coordinate system is introduced to use a meshfree approach based on the 3D degenerate shell theory for analyzing curved FSDT shell structures. This coordinate system is attached to the curved surface. A mapping technique is used to connect the global Cartesian and the local convected coordinate systems. This approach is proposed by Noguchi et al. [23]. This mapping technique can map an arbitrary 3D curved shell in the Cartesian coordinate system to a 2D space (convected coordinate system). The RPIM shape function is then used to interpolate the curved

**Cite this article :** Truong T T, Lo V S. **Free Vibration Analysis of Curved Shell Structures with Various Boundary Conditions by Using A Meshfree Method**. *Sci. Tech. Dev. J. – Engineering and Technology* 2023 5(SI2):87-98.

History
• Received: 02-05-2023
• Accepted: 30-8-2023
• Published Online: 31-12-2023

DOI :
https://doi.org/10.32508/stdjet.v6iSI6.1097



shell geometry and the field variables in the 2D space. The solution is obtained by mapping the computation in the convected coordinate system back to the 3D space.

The meshfree method based on RPIM shape function is used in this paper to analyze the free vibration behavior of different curved shell structures with arbitrary boundary conditions. The FSDT curved shell is formulated using the 3D degenerate shell theory with the mapping technique. The quartic function is used as the radial basis to construct the RPIM shape function and the polynomial basis is the second-order polynomial.

The paper is organized as follows. Section 2 gives a brief on the theory of shell structures: curved shell kinematics, the constitutive equation for isotropic homogeneous material and the discrete equation for free vibration analysis. Section 3 investigates numerical examples with various geometries and boundary conditions to show the accuracy of the RPIM approach in analyzing the free vibration of curved shells. Section 4 presents some discussions based on the obtained results. The last Section gives some conclusions and outlooks.

# METHODOLOGY

## Kinematics of Shell

Considering two vectors $X = (x_1, x_2, x_3)$ and $r = (r^1, r^2, r^3)$, in that order, are the position vector in the global Cartesian and the local convected coordinate system. The two coordinate systems are shown in Figure 1.

The orthogonal unit vectors in the Cartesian and in the convected coordinate system are denoted by $e_i$ and $V_i$, respectively. The vectors $V_i$ are defined as follows: $V_3$ is a vector perpendicular to the mid-surface,

$$V_2 = \frac{V_3 \times e_1}{|V_3 \times e_1|} \text{ and } V_1 = V_2 \times V_3 \tag{1}$$

The position of a point on the curved shell based on the FSDT is defined by a vector X as the following equation[23]:

$$X = X_{mid} + \frac{r^3}{2} t V_3 \tag{2}$$

where $t$ denotes the shell thickness and the position vector of an arbitrary point located on the mid-surface of shell is expressed by the notation $X_{mid}$.

The displacement vector u of a point on the curved shell can be written in a similar way as[23]:

$$u = u_{mid} + \frac{r^3}{2} t \left(-\beta_1 V_2 + \beta_2 V_1\right) \tag{3}$$

where $u_{mid} = [u_{mid1}, u_{mid2}, u_{mid3}]^T$ is the translation of an arbitrary point on the mid-surface, $\beta_1$ and $\beta_2$ are the rotation angles about $V_1$ and $V_2$, respectively.

## Constitutive Equation

First, the covariant and contravariant base vectors of the convected coordinate system are presented as following. The covariant base vectors are computed as below

$$G_i = \frac{\partial X}{\partial r_i} \tag{4}$$

and from the above equation, the contravariant base vectors can be defined by the relation

$$G^i = \frac{G_j \times G_k}{[G_1 G_2 G_3]} \tag{5}$$

in which $\left[G_i G_j G_k\right] = G_i \times G_j . G_k$ is called the scalar triple product.

Now, the following expression defines the linear strain-displacement relationship using the covariant and contravariant base vectors[23]

$$\begin{aligned} \varepsilon &= \frac{1}{2}\left(G_i \frac{\partial u}{\partial r^j}\right) + G_j \frac{\partial u}{\partial r^i} G^i \otimes G^j \\ &= \varepsilon_{ij} G^i \otimes G^j \end{aligned} \tag{6}$$

The constitutive equation is given as the following equation

$$\sigma = C : \varepsilon \tag{7}$$

where

$$\sigma = \sigma^{ij} G_i \otimes G_j \tag{8}$$

is the Cauchy stress, and the fourth-order constitutive tensor C is defined as

$$C = C^{ijkl} G_i \otimes G_j \otimes G_k \otimes G_l \tag{9}$$

in which

$$\begin{aligned} &C^{ijkl} = \\ &C_{mnop}\left(V_m \cdot G^i\right)\left(V_n \cdot G^j\right)\left(V_o \cdot G^k\right)\left(V_p \cdot G^l\right) \end{aligned} \tag{10}$$

and the covariant coefficient matrix $C_{ijkl}$ is given as[24]

$$\begin{aligned} C_{ijkl} &= \begin{bmatrix} C_{1111} & C_{1122} & C_{1112} & C_{1123} & C_{1131} \\ C_{2211} & C_{2222} & C_{2212} & C_{2223} & C_{2231} \\ C_{1211} & C_{1222} & C_{1212} & C_{1223} & C_{1231} \\ C_{2311} & C_{2322} & C_{2312} & C_{2323} & C_{2331} \\ C_{3111} & C_{3122} & C_{3112} & C_{3123} & C_{3131} \end{bmatrix} \\ &= \frac{E}{1-\nu^2} \begin{bmatrix} 1 & \nu & 0 & 0 & 0 \\ & 1 & 0 & 0 & 0 \\ & & \frac{1-\nu}{2} & 0 & 0 \\ & & & \kappa\frac{1-\nu}{2} & 0 \\ sym. & & & & \kappa\frac{1-\nu}{2} \end{bmatrix} \end{aligned} \tag{11}$$

where E denotes Young's modulus, $\nu$ is Poisson ratio and the shear correction factor often takes the value $\kappa = 5/6$[14].

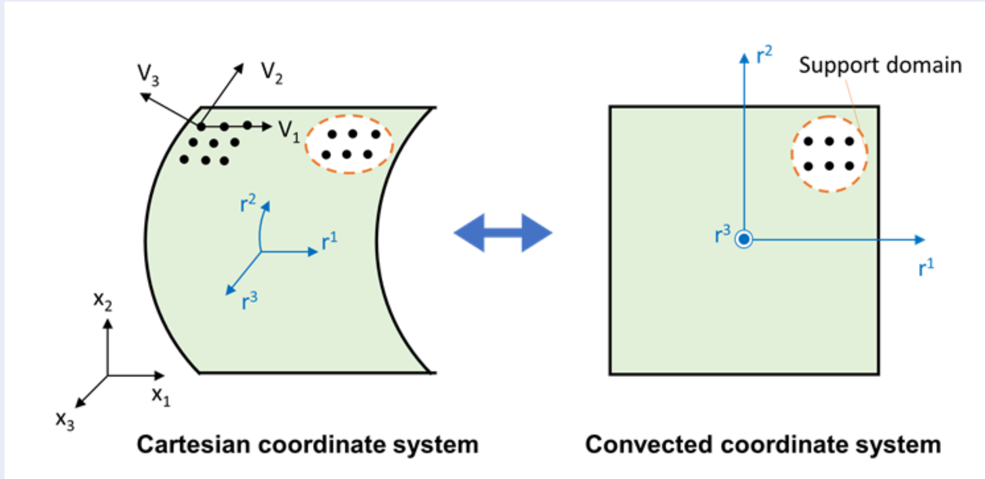


**Figure 1**: Illustration of the Cartesian and convected coordinate systems.

## Discrete Form of Free Vibration Equation

The shape function in this study is derived from the radial point interpolation method (RPIM). A radial basis and a polynomial basis are used to construct the RPIM shape function $\phi_I$.

The radial basis used in this study is the quartic function due to its stability to the change of shape parameter $\theta$

$$R_I(x) = 1 - 6\left(\frac{\theta}{l_s}\right)^2 r_I^2 + 8\left(\frac{\theta}{l_s}\right)^3 r_I^3 - 3\left(\frac{\theta}{l_s}\right)^4 r_I^4 \quad (12)$$

where $r_I$ is the distance between the node $x_I$ and the point of interest x, $l_s$ is the maximum distance between any pair of nodes.

And the second-order polynomial is used as the polynomial basis because of its high accuracy and low computational cost. More detail on the step-by-step formulation of the RPIM shape function can be found in the reference [30].

The discrete form of the position vector X($r$) is given as following

$$X = \Sigma_{I=1}^{N} \phi_I\left(r^1, r^2\right)\left(X_I + \frac{r^3}{2} t V_{13}\right) \quad (13)$$

where the RPIM shape function $\phi_I\left(r^1, r^2\right)$ is computed on the convected coordinate.

The orthogonal unit vectors V$_i$ in Eq. (1) are calculated as the following expression

$$V_i = \frac{\sum_{I=1}^{N} \phi_I\left(r^1, r^2\right) V_{Ii}}{\left|\Sigma_{I=1}^{N} \phi_I\left(r^1, r^2\right) V_{Ii}\right|} \; (i = 2, 3) \quad (14)$$

$$V_1 = V_2 \times V_3 \quad (15)$$

From the definition in Eq. (4) and the position vector in Eq. (13), the covariant bases vectors are defined as

$$G_i = \Sigma_{I=1}^{N} \frac{\partial \phi_I\left(r^1, r^2\right)}{\partial r^i}\left(X_I + \frac{r^3}{2} t V_{I3}\right) \; (i = 1, 2) \quad (16)$$

$$G_3 = \Sigma_{I=1}^{N} \frac{1}{2} \phi_I\left(r^1, r^2\right) t V_{I3} \quad (17)$$

The dynamic equation for free vibration is

$$M\ddot{U} + KU = 0 \quad (18)$$

where the vector contains all nodal degrees of freedom (DOFs). And it has five DOFs at each node $[u_{mid1}\; u_{mid2}\; u_{mid3}\; \beta_1\; \beta_2]^T$.

The stiffness matrix and mass matrix are derived as the following equations [26]

$$K = \int_{r^1}\int_{r^2}\int_{r^3} B^T C B \left[G_1 G_2 G_3\right] dr^1 dr^2 dr^3 \quad (19)$$

$$M = \int_{r^1}\int_{r^2}\int_{r^3} \rho N^T N \left[G_1 G_2 G_3\right] dr^1 dr^2 dr^3 \quad (20)$$

where $\rho$ is the density.

The shape function matrix N in Eq. (20) and strain-computing matrix B in Eq. (19) are expressed as

$$N = \begin{bmatrix} \phi & 0 & 0 & -\frac{t}{2} r^3 \phi (V_2)_1 & \frac{t}{2} r^3 \phi (V_2)_1 \\ 0 & \phi & 0 & -\frac{t}{2} r^3 \phi (V_2)_2 & \frac{t}{2} r^3 \phi (V_2)_2 \\ 0 & 0 & \phi & -\frac{t}{2} r^3 \phi (V_2)_3 & \frac{t}{2} r^3 \phi (V_2)_3 \end{bmatrix} \quad (21)$$

$$B = \left[\begin{array}{ccc} G_1 a_{11} & G_1 a_{12} & G_1 a_{13} \\ G_2 a_{21} & G_2 a_{22} & G_2 a_{23} \\ G_1 a_{21} + G_2 a_{11} & G_1 a_{22} + G_2 a_{12} & G_1 a_{23} + G_2 a_{13} \\ G_3 a_{21} & G_3 a_{22} & G_3 a_{23} \\ G_3 a_{11} & G_3 a_{12} & G_3 a_{13} \\ & G_1 b_{11} & G_1 b_{12} \\ & G_2 b_{21} & G_2 b_{22} \\ & G_1 b_{21} + G_2 b_{11} & G_1 b_{22} + G_2 b_{12} \\ & G_3 b_{21} + G_2 c_1 & G_3 b_{22} + G_2 c_2 \\ & G_3 b_{11} + G_1 c_1 & G_3 b_{12} + G_1 c_2 \end{array}\right] \quad (22)$$

in which the bracket and subscript "i" $(\,)_i$ indicate the ith component of the vector, and $\phi$ is the vector containing all the shape function .

The coefficient $\begin{bmatrix} a_{i1} & a_{i2} & a_{i3} \end{bmatrix}$, $\begin{bmatrix} b_{i1} & b_{i2} \end{bmatrix}$ and $\begin{bmatrix} c_1 & c_2 \end{bmatrix}$ are expressed as

$$\begin{bmatrix} a_{i1} & a_{i2} & a_{i3} \end{bmatrix} = \begin{bmatrix} \frac{\partial \phi}{\partial r^i} & 0 & 0 \\ 0 & \frac{\partial \phi}{\partial r^i} & 0 \\ 0 & 0 & \frac{\partial \phi}{\partial r^i} \end{bmatrix} \quad (23)$$

$[\mathrm{b}_{i1}\ \mathrm{b}_{i2}] =$

$$\begin{bmatrix} -\frac{r^3}{2} t \left\{ (V_2)_1 \frac{\partial \phi}{\partial r^i} + \left( \frac{\partial V_2}{\partial r^i} \right)_1 \phi \right\} & \frac{r^3}{2} t \left\{ (V_2)_1 \frac{\partial \phi}{\partial r^i} + \right. \\ -\frac{r^3}{2} t \left\{ (V_2)_2 \frac{\partial \phi}{\partial r^i} + \left( \frac{\partial V_2}{\partial r^i} \right)_2 \phi \right\} & \frac{r^3}{2} t \left\{ (V_2)_2 \frac{\partial \phi}{\partial r^i} + \right. \\ -\frac{r^3}{2} t \left\{ (V_2)_3 \frac{\partial \phi}{\partial r^i} + \left( \frac{\partial V_2}{\partial r^i} \right)_3 \phi \right\} & \frac{r^3}{2} t \left\{ (V_2)_3 \frac{\partial \phi}{\partial r^i} + \right. \end{bmatrix}$$

$$\begin{bmatrix} c_1 & c_2 \end{bmatrix} = \begin{bmatrix} -\frac{1}{2} t (V_2)_1 \phi & \frac{1}{2} t (V_2)_1 \phi \\ -\frac{1}{2} t (V_2)_2 \phi & \frac{1}{2} t (V_2)_2 \phi \\ -\frac{1}{2} t (V_2)_3 \phi & \frac{1}{2} t (V_2)_3 \phi \end{bmatrix} \quad (25)$$

$$\frac{\partial V_i}{\partial r^j} = (I - V_i \otimes V_i) \frac{\sum_{I=1}^{N} \frac{\partial \phi_I}{\partial r^j} V_{Ii}}{\left| \sum_{I=1}^{N} \frac{\partial \phi_I}{\partial r^j} V_{Ii} \right|} \quad (26)$$

$(i = 2, 3;\ j = 1, 2)$

$$\frac{\partial V_1}{\partial r^j} = \frac{\partial V_2}{\partial r^j} \times V_3 + V_2 \times \frac{\partial V_3}{\partial r^j} \ (j = 1, 2) \quad (27)$$

The natural frequency/eigenvalue ($\omega$) and the mode shape/eigenvector ($\bar{u}$) can be obtained by solving the eigenvalue equation form of Eq. (18)

$$\left( K - \omega^2 M \right) \bar{u} = 0 \quad (28)$$

## RESULTS

Three numerical examples are conducted in this section, particularly:

- Validation and convergence of the meshfree method for free vibration analysis of flat shell structures,
- Free vibration analysis of the open cylindrical shell with various boundary conditions, and
- Free vibration analysis of the open spherical shell with various boundary conditions.

Three basic types of boundary conditions used in the study are abbreviated as follows: C – Clamped or Fixed supported, S – Simply supported, and F – Free. The natural frequencies are evaluated in each problem and compared with other reliable references.

### Convergence and Validation

In this first example, a fully clamped square flat shell of side a = 1 $m$ is examined, see Figure 2. The flat shell in this test has the thickness t = 0.1 m. The material properties are: Young's modulus E = 210 GPa, Poisson ratio $v = 0.3$ and the density $\rho = 7800\ kg/m^3$. The non-dimensional frequency $\bar{\omega} = \omega a \sqrt{\frac{\rho}{G}}$ is considered, where $G$ is the shear modulus. The obtained results from the present study is compared with Rayleigh-Ritz method[31] and the RKPM[32].

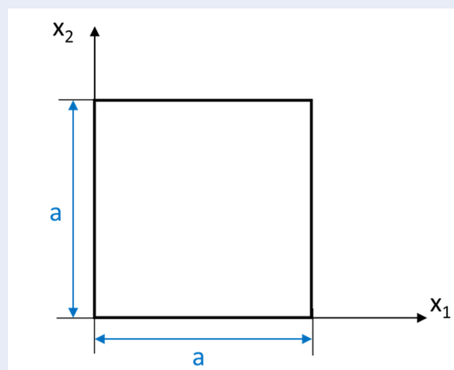


Figure 2: Geometry of the square flat shell.

Five different discrete models are used in the convergence study: $7 \times 7$, $9 \times 9$, $11 \times 11$, $13 \times 13$ and $15 \times 15$ nodes. The convergence rate of the non-dimensional frequency is shown in Figure 3. It is observed from the figure that the convergence rate of the RPIM method is rapid, the RPIM results are high accuracy despite a coarse discretization. Therefore, the discrete model of $15 \times 15$ nodes is then used for the next examination.

**Table 1: Non-dimensional frequencies of the CCCC square flat shell (the first five modes)**

| | RPIM | Rayleigh-Ritz [31] | RKPM [32] |
|---|---|---|---|
| Mode 1 | 1.5990 | 1.5940 | 1.5582 |
| Mode 2 | 3.0547 | 3.0390 | 3.0182 |
| Mode 3 | 3.0547 | 3.0390 | 3.0182 |
| Mode 4 | 4.3253 | 4.2650 | 4.1711 |
| Mode 5 | 5.0397 | 5.0350 | 5.1218 |

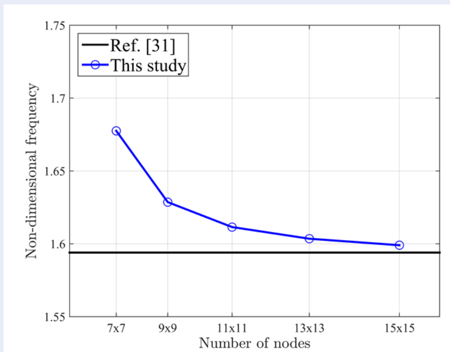


**Figure 3**: Convergence of mode 1 non-dimensional frequency.

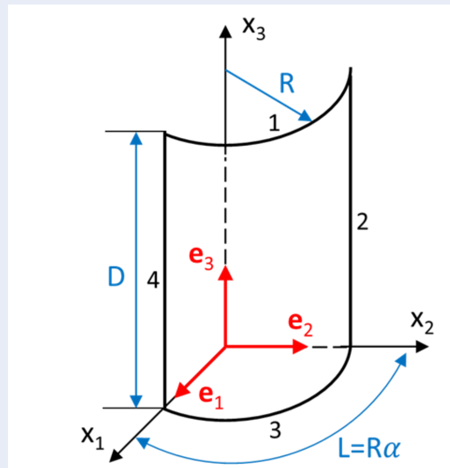


**Figure 4**: Geometry of the open cylindrical shell.

Table 1 shows the first five non-dimensional frequencies obtained by RPIM compared to other methods. It is seen that the results obtained in this study show good agreement with other approaches. This means that using the RPIM meshfree method for free vibrations analysis of the curved shell (as described in section 2) is utterly appropriate.

## An open cylindrical shell

An open cylindrical shell is considered in this example, see Figure 4. The dimensions of the shell are described as follows: R = 2 m, D = 1 m, $\alpha = 0.5$ *rad* and t = 0.05 m. Material properties are given as follows: E = 210 GPa, $\nu = 0.3$ and the density $\rho = 7800\ kg/m^3$. The discrete model of the cylindrical shell is a set of $15 \times 15$ scattered nodes, see Figure 5. The non-dimensional frequency $\bar{\omega} = \omega D^2 \sqrt{\frac{\rho t}{D_{fs}}}$ is considered, $D_{fs}$ is the flexural stiffness $D_{fs} = \frac{Et^3}{12(1-\nu^2)}$. Many combinations of boundary conditions are examined, the order of edges when applying boundary conditions is numbered 1-2-3-4 in Figure 4.

Table 2 shows the dimensionless frequencies of the open cylindrical shell obtained in this study and from the Spectro-Geometric-Ritz Method[33]. The obtained results show a high similarity between the two methods. It is also observed that the CFFF case has the

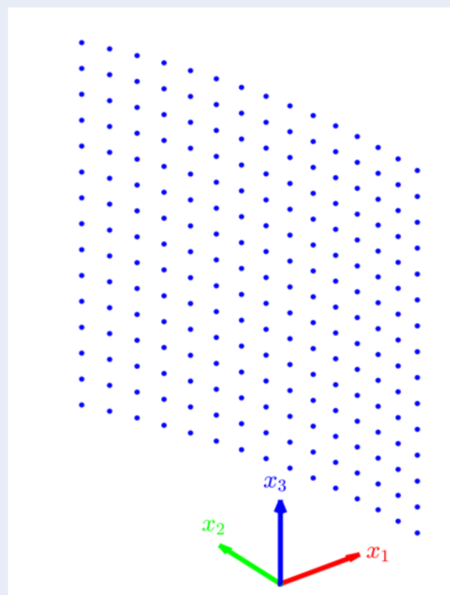


**Figure 5**: Discrete model ($15 \times 15$ nodes) of the open cylindrical shell

**Table 2: Non-dimensional frequencies of the open cylindrical shell with various boundary conditions (the first four modes)**

| BC | RPIM | | | |
|---|---|---|---|---|
| | 1 | 2 | 3 | 4 |
| CCCC | 46.35 | 74.26 | 77.31 | 108.68 |
| | 25.51 | 49.84 | 55.11 | 79.59 |
| CCCS | 37.78 | 63.90 | 73.67 | 100.06 |
| CSCS | 33.46 | 55.51 | 71.54 | 93.80 |
| CCSS | 33.98 | 61.15 | 65.17 | 92.84 |
| CSSS | 28.95 | 52.34 | 62.84 | 86.22 |
| CCCF | 27.80 | 43.69 | 65.54 | 76.41 |
| SSSF | 16.21 | 30.24 | 46.21 | 61.36 |
| CFFF | 5.37 | 9.63 | 24.96 | 28.67 |
| BC | Spectro-Geometric-Ritz Method [33] | | | |
| | 1 | 2 | 3 | 4 |
| CCCC | 46.14 | 74.11 | 79.14 | 109.95 |
| | 25.32 | 49.34 | 55.71 | 80.23 |
| CCCS | 38.05 | 64.30 | 76.14 | 102.33 |
| CSCS | 33.66 | 55.13 | 74.00 | 95.75 |
| CCSS | 34.07 | 61.55 | 66.48 | 94.48 |
| CSSS | 28.90 | 51.86 | 64.08 | 87.38 |
| CCCF | 26.65 | 43.41 | 65.87 | 77.14 |
| SSSF | 14.82 | 29.35 | 44.94 | 61.66 |
| CFFF | 5.18 | 8.59 | 24.60 | 28.01 |

lowest frequency and the fully clamped case (CCCC) has the highest natural frequency. This is as expected since the CCCC case has more constraints than the CFFF case so it is harder for the cylindrical shell to vibrate. The same observation for the frequency of CCCF and SSSF since CCCF has more constraints. For the case of CSCS and CCSS the frequencies of modes 1 and 4 are approximately the same. Whereas modes 2 and 3 are different, maybe because the locations of the "C" and "S" constraints are different.

Figure 6 shows the mode shapes of four lowest modes of the CCCF cylindrical shell. The colormap used in the figure is the value of eigenvectors in the $x_1$ direction.

## An open spherical shell

In this example, an open spherical shell is considered. The dimensions of the shell are described as follows: R = 2 m, $\alpha_1 = 0.5\ rad$, $\alpha_2 = 0.5\ rad$ and t = 0.05 m, see Figure 7. This example also using isotropic material with the properties are: Young's modulus E = 70 GPa, Poisson ratio $v = 0.3$ and the density $\rho = 2700\ kg/m^3$. The spherical shell is discretized into a set of $15 \times 15$ scattered nodes, see Figure 8. The non-dimensional frequency $\bar{\omega} = \omega D^2 \sqrt{\frac{\rho t}{D_{fs}}}$ is considered. Various boundary conditions are examined, the order of edges when applying boundary conditions is numbered 1-2-3-4 in Figure 7.

Table 3 shows the non-dimensional frequencies of the open spherical shell obtained in this study and from the Ritz Method [34]. The obtained results show a good agreement between the two methods. Similar to the open cylindrical shell, it is also observed that the CFFF case has the lowest frequency and the CCCC case has the highest natural frequency. And the same observation for the frequency of CCCF and SSSF since CCCF has more constraints. For the case of CSCS and CCSS, this is a little bit different from the cylindrical

**Table 3: Non-dimensional frequencies of the open spherical shell with various boundary conditions (the first four modes)**

| BC | RPIM | | | |
|---|---|---|---|---|
| | 1 | 2 | 3 | 4 |
| CCCC | 58.66 | 79.60 | 81.80 | 114.09 |
| | 38.41 | 59.17 | 60.72 | 86.85 |
| CCCS | 50.31 | 73.42 | 76.76 | 106.46 |
| CSCS | 46.85 | 65.63 | 74.79 | 100.13 |
| CCSS | 44.22 | 68.43 | 70.12 | 98.99 |
| CSSS | 41.01 | 62.25 | 66.32 | 92.40 |
| CCCF | 37.47 | 55.03 | 62.67 | 84.95 |
| SSSF | 13.33 | 42.98 | 43.16 | 65.03 |
| CFFF | 4.34 | 7.94 | 21.29 | 27.37 |
| BC | Ritz Method [34] | | | |
| | 1 | 2 | 3 | 4 |
| CCCC | 58.04 | 80.84 | 80.92 | 112.54 |
| | 38.01 | 59.10 | 59.10 | 85.32 |
| CCCS | 50.51 | 72.22 | 78.62 | 106.22 |
| CSCS | 46.87 | 64.10 | 76.80 | 100.07 |
| CCSS | 44.57 | 69.21 | 69.78 | 98.39 |
| CSSS | 41.28 | 61.27 | 67.58 | 92.35 |
| CCCF | 37.96 | 55.15 | 65.22 | 83.90 |
| SSSF | 13.14 | 42.40 | 44.25 | 64.32 |
| CFFF | 4.72 | 8.39 | 22.09 | 28.80 |

shell. The discrepancy in the two cases is larger, but the frequencies of all four modes are relatively similar.

Figure 9 shows the mode shapes of four lowest modes of the CFFF spherical shell. The colormap used in the figure is the value of eigenvectors in the $x_1$ direction.

## DISCUSSIONS

The approach in Section 2 is shown to be suitable for the free vibration analysis of curved shells by the obtained results, which agree well with those from other numerical methods, as presented in Section 3.

For the convergence and validation test, the obtained results show good agreement with the RKPM and the Rayleigh-Ritz method. The convergence rate of the RPIM method is rapid and the RPIM results are high accuracy despite a coarse discretization.

For the cylindrical shell example, the obtained results show a high similarity between RPIM and the Spectro-Geometric-Ritz methods. It is also observed that the CFFF case has the lowest frequency and the CCCC case has the highest natural frequency. This is as expected since the CCCC case has more constraints than the CFFF case so it is harder for the cylindrical shell to vibrate. The same observation for the frequency of CCCF and SSSF since CCCF has more constraints. For the case of CSCS and CCSS the frequencies of modes 1 and 4 are approximately the same. Whereas modes 2 and 3 are different, maybe because the locations of the “C” and “S” constraints are different.

Good agreement is observed between RPIM and the Ritz methods in the spherical shell example. Similar to the open cylindrical shell, it is also observed that the CFFF case has the lowest frequency and the CCCC case has the highest natural frequency. And the same

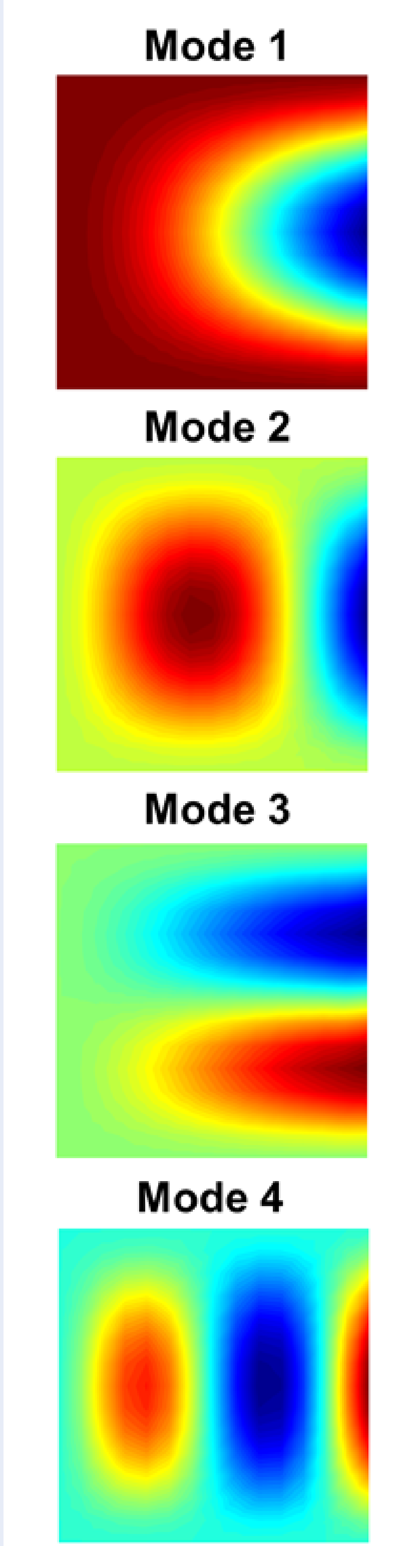


**Figure 6**: Four first modes of the CCCF cylindrical shell.

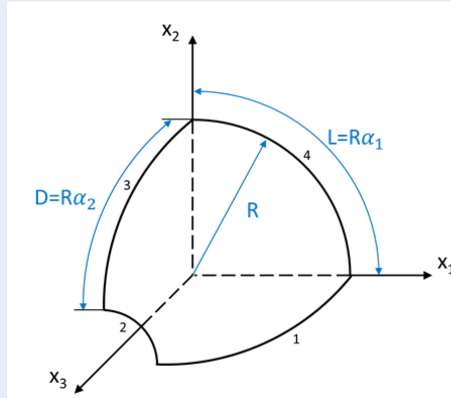


**Figure 7**: Geometry of the open spherical shell.

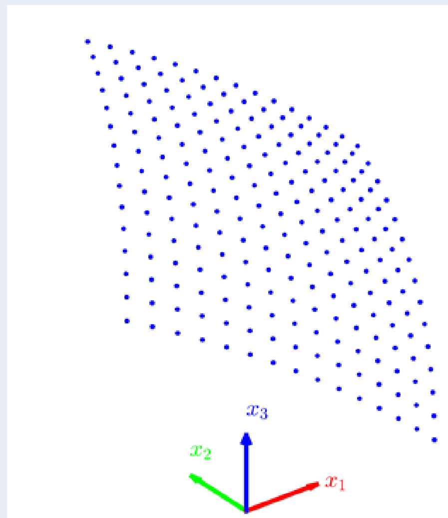


**Figure 8**: Discrete model ($15 \times 15$ nodes) of the open spherical shell.

observation for the frequency of CCCF and SSSF. For the case of CSCS and CCSS, this is a little bit different from the cylindrical shell. The discrepancy in the two cases is larger, but the frequencies of all four modes are relatively similar.

## CONCLUSIONS

The free vibration analysis of curved shell structures has been done in this paper by using the meshfree method based on RPIM. The shell structures are modeled using the 3D degenerate shell theory, and the shell formulation is based on the first-order shear deformation theory. The FSDT is a straightforward shell formulation requiring only $C^0$ continuity. The RPIM is a meshfree method that has the Kronecker

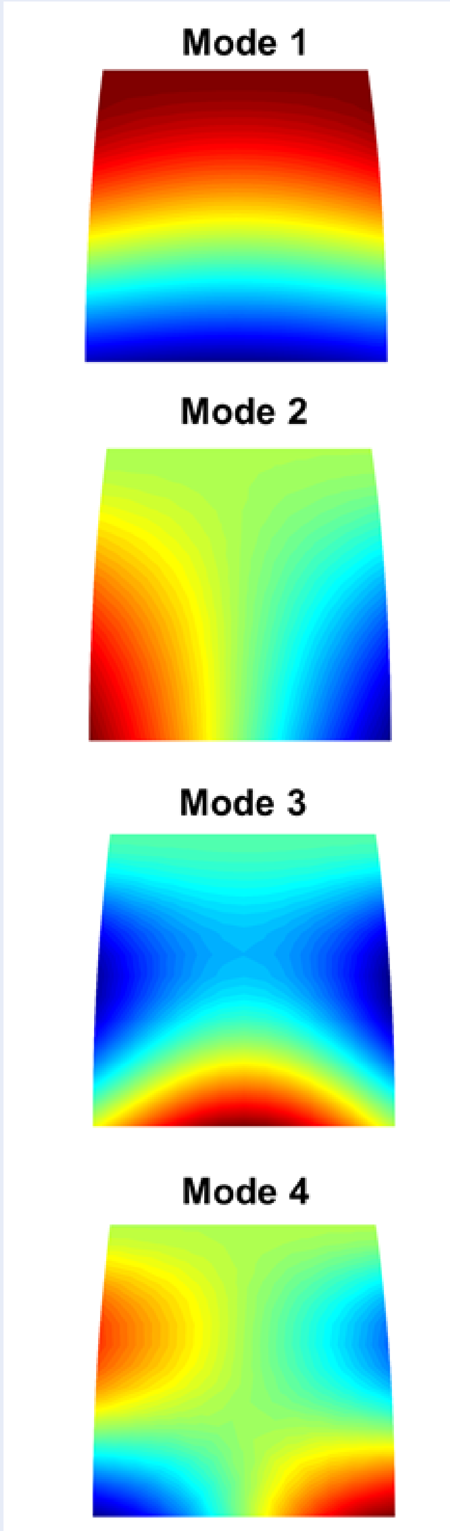


**Figure 9**: Four first modes of the CFFF spherical shell.

delta property. This property enables RPIM to impose essential boundary conditions directly, which is not possible for other meshfree methods. A mapping technique is employed to connect the global Cartesian and the local convected coordinate systems. The geometry of the curved shell and the field variables in the convected coordinate are interpolated by the meshfree RPIM shape function. The solution of the problem is obtained by mapping the computation in the convected coordinate system back to the 3D space. The present approach is shown to be accurate through many numerical examples. Good agreement with the solution from other numerical methods is observed.

## ACKNOWLEDGMENT

This research is funded by Vietnam National University Ho Chi Minh City (VNU-HCM) under grant number B2023-20-03. We acknowledge Ho Chi Minh City University of Technology (HCMUT), VNU-HCM for supporting this study.

## ABBREVIATIONS

EFG: Element-Free Galerkin
DOF: Degree Of Freedom
FEM: Finite Element Method
FSDT: First-order Shear Deformation Theory
MK: Moving Kriging
RKPM: Reproducing Kernel Particle Method
RPIM: Radial Point Interpolation Method

## CONFLICT OF INTEREST

Group of authors declare that this manuscript is original, has not been published before and there is no conflict of interest in publishing the paper.

## AUTHORS' CONTRIBUTION

Thien Tich Truong is the supervisor, he also contributes ideas for the proposed method.
Vay Siu Lo works as the developer of the method and the manuscript editor.

## REFERENCES


1. Aksu T. A finite element formulation for free vibration analysis of shells of general shape. Comput Struct. 1997;65(5):687-94;Available from: https://doi.org/10.1016/S0045-7949(96)00423-3.
2. Pham TD, Pham QH, Phan VD, Nguyen HN, Do VT. Free vibration analysis of functionally graded shells using an edge-based smoothed finite element method. Symmetry. 2019;11(5):684;Available from: https://doi.org/10.3390/sym11050684.
3. Rawat A, Matsagar VA, Nagpal AK. Free vibration analysis of thin circular cylindrical shell with closure using finite element method. Int J Steel Struct. 2020;20(1):175-93;Available from: https://doi.org/10.1007/s13296-019-00277-5.
4. Tuan TA, Quoc TH, Tu TM. Free vibration analysis of laminated stiffened cylindrical panels using finite element method. Viet J Sci Technol. 2016;54(6):771-84;Available from: https://doi.org/10.15625/0866-708X/54/6/8214.
5. Huan DT, Quoc TH, Tu TM. Free vibration analysis of functionally graded shell panels with various geometric shapes in thermal environment. Viet J Mech. 2018;40(3):199-215;Available from: https://doi.org/10.15625/0866-7136/10776.
6. Menaa M, Lakis AA. Free vibration of spherical shells using a hybrid finite element method. Int J Struct Stab Dyn. 2015;15(4):1450062;Available from: https://doi.org/10.1142/S021945541450062X.
7. Mahmure A, Tornabene F, Dimitri R, Kuruoglu N. Free vibration of thin-walled composite shell structures reinforced with uniform and linear carbon nanotubes: effect of the elastic foundation and nonlinearity. Nanomaterials (Basel). 2021;11(8):2090;PMID: 34443919. Available from: https://doi.org/10.3390/nano11082090.
8. Liu T, Wang A, Wang Q, Qin B. Wave based method for free vibration characteristics of functionally graded cylindrical shells with arbitrary boundary conditions. Thin Wall Struct. 2020;148:106580;Available from: https://doi.org/10.1016/j.tws.2019.106580.
9. Zhao J, Choe K, Shuai C, Wang A, Wang Q. Free vibration analysis of laminated composite elliptic cylinders with general boundary conditions. Compos B Eng. 2019;158:55-66;Available from: https://doi.org/10.1016/j.compositesb.2018.09.009.
10. Tang D, Wu G, Yao X, Wang C. Free vibration analysis of circular cylindrical shells with arbitrary boundary conditions by the method of reverberation-ray Matrix. Shock Vib. 2016;2016:1-18;Available from: https://doi.org/10.1155/2016/3814693.
11. Hughes TJR, Tezduyar TE. Finite elements based upon mindlin plate theory with particular reference to the four-node bilinear isoparametric element. J Appl Mech. 1981;48(3):587-96;Available from: https://doi.org/10.1115/1.3157679.
12. Ye X, Zhang S, Zhang Z. A locking-free weak galerkin finite element method for reissner-mindlin plate on polygonal meshes. Comput Math Appl. 2020;80(5):906-16;Available from: https://doi.org/10.1016/j.camwa.2020.05.015.
13. Bitar I, Richard B. Mindlin-reissner plate formulation with enhanced kinematics: theoretical framework and numerical applications. Eng Fract Mech. 2020;225:106839;Available from: https://doi.org/10.1016/j.engfracmech.2019.106839.
14. Truong TT, Lo VS, Nguyen MN, Nguyen NT, Nguyen KD. A novel meshfree radial point interpolation method with discrete shear gap for nonlinear static analysis of functionally graded plates. Eng Comput. 2023;39(4):2989-3009;Available from: https://doi.org/10.1007/s00366-022-01691-w.
15. Belinha J, Dinis LMJS. Analysis of plates and laminates using the elementfree Galerkin method. Comput Struct. 2006;84(22-23):1549-59;Available from: https://doi.org/10.1016/j.compstruc.2006.01.013.
16. Tanaka S, Suzuki H, Sadamoto S, Imachi M, Bui TQ. Analysis of cracked shear deformable plates by an effective meshfree plate formulation. Eng Fract Mech. 2015;144:142-57;Available from: https://doi.org/10.1016/j.engfracmech.2015.06.084.
17. Bui TQ, Nguyen MN, Zhang C. Buckling analysis of Reissner-Mindlin plates subjected to in-plane edge loads using a shear-locking-free and meshfree method. Eng Anal Bound Elem. 2011;35(9):1038-53;Available from: https://doi.org/10.1016/j.enganabound.2011.04.001.
18. Bui TQ, Doan DH, Van Do T, Hirose S, Duc ND. High frequency modes meshfree analysis of Reissner-Mindlin plates. J Sci Adv Mater Dev. 2016;1(3):400-12;Available from: https://doi.org/10.1016/j.jsamd.2016.08.005.
19. Wang JG, Liu GR. A point interpolation meshless method based on radial basis functions. Int J Numer Methods Eng. 2002;54(11):1623-48;Available from: https://doi.org/10.1002/nme.489.
20. Liew KM, Chen XL. Mesh-free radial point interpolation method for the buckling analysis of Mindlin plates subjected to in-plane point loads. Int J Numer Methods Eng. 2004;60(11):1861-77;Available from: https://doi.org/10.1002/nme.1027.
21. Simo JC, Fox DD, Rifai MS. Formulation and computational aspects of a stress resultant geometrically exact shell model. Comput Mech. 1988;88:751-9;Available from: https://doi.org/10.1007/978-3-642-61381-4_192.
22. Krysl P, Belytschko T. Analysis of thin shells by the Element-Free Galerkin method. Int J Solids Struct. 1996;33(20-22):3057-80;Available from: https://doi.org/10.1016/0020-7683(95)00265-0.
23. Noguchi H, Kawashima T, Miyamura T. Element free analyses of shell and spatial structures. Int J Numer Methods Eng. 2000;47(6):1215-40;Available from: https://doi.org/10.1002/(SICI)1097-0207(20000228)47:6<1215::AID-NME834>3.0.CO;2-M.
24. Dai MJ, Tanaka S, Sadamoto S, Yu T, Bui TQ. Advanced reproducing kernel meshfree modeling of cracked curved shells for mixed-mode stress resultant intensity factors. Eng Fract Mech. 2020;233:107012;Available from: https://doi.org/10.1016/j.engfracmech.2020.107012.
25. Peng YX, Zhang AM, Ming FR. A 3D meshfree crack propagation algorithm for the dynamic fracture in arbitrary curved shell. Comput Methods Appl Mech Eng. 2020;367:113-39;Available from: https://doi.org/10.1016/j.cma.2020.113139.
26. Chen W, Luo WM, Chen SY, Peng LX. A FSDT meshfree method for free vibration analysis of arbitrary laminated composite shells and spatial structures. Compos Struct. 2022;279:114763;Available from: https://doi.org/10.1016/j.compstruct.2021.114763.
27. Sadamoto S, Tanaka S, Taniguchi K, Ozdemir M, Bui TQ, Murakami C. Buckling analysis of stiffened plate structures by an improved meshfree flat shell formulation. Thin Wall Struct. 2017;117:303-13;Available from: https://doi.org/10.1016/j.tws.2017.04.012.
28. Sadamoto S, Ozdemir M, Tanaka S, Taniguchi K, Yu TT, Bui TQ. An effective meshfree reproducing kernel method for buckling analysis of cylindrical shells with and without cutouts. Comput Mech. 2017;59(6):919-32;Available from: https://doi.org/10.1007/s00466-017-1384-5.
29. Sadamoto S, Ozdemir M, Tanaka S, Bui TQ, Okazawa S. Finite rotation meshfree formulation for geometrically nonlinear analysis of flat, curved and folded shells. Int J Non Linear Mech. 2020;119:103300;Available from: https://doi.org/10.1016/j.ijnonlinmec.2019.103300.
30. Liu GR. Meshfree methods: moving beyond the finite element method. Boca Raton: CRC Press; 2010;.
31. Dawe DJ, Roufaeil OL. Rayleigh-ritz vibration analysis of mindlin plates. J Sound Vib. 1980;69(3):345-59;Available from: https://doi.org/10.1016/0022-460X(80)90477-0.
32. Liew KM, Wang J, Ng TY, Tan MJ. Free vibration and buckling analyses of shear-deformable plates based on FSDT meshfree method. J Sound Vib. 2004;276(3-5):997-1017;Available from: https://doi.org/10.1016/j.jsv.2003.08.026.
33. Shi D, Zhao Y, Wang Q, Teng X, Pang F. A unified Spectro-geometric-ritz method for vibration analysis of open and

closed shells with arbitrary boundary conditions. Shock Vib. 2016;2016:1-30;Available from: https://doi.org/10.1155/2016/4097123.

34. Qatu MS, Asadi E. Vibration of doubly curved shallow shells with arbitrary boundaries. Appl Acoust. 2012;73(1):21-7;Available from: https://doi.org/10.1016/j.apacoust.2011.06.013.

*Tạp chí Phát triển Khoa học và Công nghệ – Engineering and Technology 2023, 5(SI2):87-98*

Open Access Full Text Article

*Bài nghiên cứu*

# Phân tích dao động tự do của các kết cấu dạng vỏ cong với các điều kiện biên khác nhau bằng phương pháp không lưới

**Trương Tích Thiện[1,2,*], Lồ Sìu Vẫy[1,2]**

**TÓM TẮT**

Trong bài báo này, dao động tự do của các kết cấu vỏ cong với các điều kiện biên khác nhau được khảo sát bằng phương pháp không lưới. Phương pháp không lưới trong nghiên cứu này dựa trên phương pháp nội suy điểm hướng kính (RPIM). Hàm dạng RPIM được chọn vì nó thỏa mãn thuộc tính Kronecker delta cho phép áp đặt trực tiếp các điều kiện biên cần thiết. Các biến trường và dạng hình học của vỏ cong được nội suy thông qua hàm dạng RPIM. Công thức vỏ cong được xây dựng dựa trên lý thuyết biến dạng trượt bậc nhất (FSDT), có xét đến biến dạng trượt. Trong phương pháp không lưới để khảo sát các kết cấu vỏ cong, một hệ tọa độ đối lưu được sử dụng. Hệ tọa độ này được gắn vào bề mặt cong và được sử dụng để ánh xạ một vỏ cong tùy ý trong không gian 3 chiều (hệ tọa độ tổng thể) vào không gian 2 chiều (hệ tọa độ đối lưu). Việc tính toán trước hết được tiến hành trong hệ tọa độ đối lưu này và sau đó được ánh xạ trở lại hệ tọa độ tổng thể để thu được kết quả. Độ chính xác và khả năng của phương pháp không lưới được thể hiện qua nhiều ví dụ số. Tần số dao động tự nhiên của các vỏ cong có dạng hình học khác nhau với các điều kiện biên khác nhau được so sánh với các tài liệu tham khảo tin cậy và cho thấy sự phù hợp tốt.

**Từ khoá:** phân tích dao động tự do, vỏ cong, FSDT, phương pháp không lưới

[1]*Bộ môn Cơ kỹ thuật, Khoa Khoa học ứng dụng, Trường Đại học Bách Khoa TP.HCM, Việt Nam*

[2]*Đại học Quốc gia Thành phố Hồ Chí Minh, Việt Nam*

**Liên hệ**

**Trương Tích Thiện**, Bộ môn Cơ kỹ thuật, Khoa Khoa học ứng dụng, Trường Đại học Bách Khoa TP.HCM, Việt Nam

Đại học Quốc gia Thành phố Hồ Chí Minh, Việt Nam

Email: tttruong@hcmut.edu.vn

**Lịch sử**

- Ngày nhận: 02-05-2023
- Ngày chấp nhận: 30-8-2023
- Ngày đăng: 31-12-2023

**DOI : https://doi.org/10.32508/stdjet.v6iSI6.1097**



**Trích dẫn bài báo này:** Thiện T T, Vẫy L S. **Phân tích dao động tự do của các kết cấu dạng vỏ cong với các điều kiện biên khác nhau bằng phương pháp không lưới**. *Sci. Tech. Dev. J. - Eng. Tech.* 2023, 5(SI2):87-98.